Journal Name

ARTICLE TYPE

Cite this: DOI: 10.1039/xxxxxxxxxx

Supplementary Information: Nanoscale depth control of implanted shallow silicon vacancies in silicon carbide†

Qiang Li,*[a,b] Jun-Feng Wang,*[a,b] Fei-Fei Yan,[a,b] Ze-Di Cheng,[a,b] Zheng-Hao Liu,[a,b] Kun Zhou,[a,b] Li-Ping Guo,[c] Xiong Zhou,[c] Wei-Ping Zhang,[c] Xiu-Xia Wang,[d] Wei Huang,[e] Jin-Shi Xu,†[a,b] Chuan-Feng Li,†[a,b] and Guang-Can Guo,[a,b]

Received Date
Accepted Date

DOI: 10.1039/xxxxxxxxxx

www.rsc.org/journalname

1 The PL and ODMR spectrums of SiC with He^+ and H_2^+ ion implantation

To verify the V_{Si} defects in SiC generated by 20 keV He^+ ion implantation with a dose of 2×10^{13} cm^{-2}, the corresponding optical and spin properties have been measured at different etched depths. Figure S1(a) shows the confocal fluorescence image of the V_{Si} defects in SiC sample before etching. The mean counts of the V_{Si} defects is about 5.2 $Mcps$. The same SiC sample is then sequentially etched with the RIE for 40 nm, 80 nm and 120 nm, respectively. The corresponding scanning images of fluorescence intensity in the same area are shown in Figures S1(b), S1(c) and S1(d), respectively, in which the fluorescence intensity and the V_{Si} defects density in the SiC sample is reduced as etched depth increases. Moreover, there is distinct boundaries in the right and upper area of each figures, even when the layer of SiC containing V_{Si} defects is almost completely etched (Figure S1(d)), which are taken as positioning marks. At room temperature (RT), the PL spectrums of the V_{Si} defects after different etched depths are detected by a grating spectrometer (Horiba, iHR550), which are shown in Figure S1(e). The black, red, blue and green solid lines correspond to the PL spectrums of SiC sample etched for 0 nm, 40 nm, 80 nm and 120 nm, respectively. Although the PL intersity decreases with the etched depth increasing, the characteristic of the PL spectrum remains unchanged at different etched depths[1,2]. We further measure the low temperature (LT, 5 K) PL spectrum of the V_{Si} defects in SiC etched for different depths, which are shown in Figure S1(f). The two characterized zero phonon lines (ZPLs) of $V1$ (861 nm) and $V2$ (915 nm) according to the two types of V_{Si} defects in SiC are obviously demonstrated in each PL spectrums[3,4]. The results further prove that the eching process does not change the ZPL of the V_{Si} defects. We also measure the time traces of PL intensity from the V_{Si} defects in the samples after different etched depths at room temperature, in which the time bin is 10 ms. No photon blinking or photon bleaching is observed during the plasma etching processes, as shown in Figure S1(g). The negatively charged ground state of the $V2$ center is a spin quartet state with $S=3/2$ exhibiting a zero field spliiting (ZFS), and $2D=70$ MHz. We further also detect the optically detected magnetic resonance (ODMR) signals of the $V2$ defects in SiC etched for different depths at room temperature, which are exhibited in Figure S1(h). The number of scans (detection time) of the ODMR signals is fixed to be 31 times, which is the same for all the samples with different etched depths. Inferred from the fittings of the ODMR data, the resonant frequencies are from 70.1 MHz to 70.4 MHz, and the full width at half maximum (FWHM) are from 12.5 MHz to 13.0 MHz, which agree with previous results[1,4]. Moreover, the contrasts of ODMR signals of V_{Si} defects are almost the same, which demonstrate that the etching process does not change the spin properties of the V_{Si} defects.

Similar verifying results are obtained for the V_{Si} defects generated by 20 keV H_2^+ ion implantation with a dose of 2×10^{13} cm^{-2}. The corresponding optical and spin properties have been measured and the results are demonstrated in Figure S2. The RT and LT PL spectrums of the V_{Si} defects before etching are shown in Fig-

[a] CAS Key Laboratory of Quantum Information, University of Science and Technology of China, Hefei, Anhui 230026, People's Republic of China.
[b] CAS Center For Excellence in Quantum Information and Quantum Physics, University of Science and Technology of China, Hefei, Anhui 230026, People's Republic of China.
[c] Key Laboratory of Artificial Micro- and Nano-structures of Ministry of Education and School of Physics and Technology, Wuhan University, Wuhan, Hubei 430072, People's Republic of China.
[d] Center for Micro- and Nanoscale Research and Fabrication , University of Science and Technology of China, Hefei, Anhui 230026, People's Republic of China.
[e] Shanghai Institute of Ceramics, Chinese Academy of Sciences, Shanghai 201800, People's Republic of China.
* These authors contributed equally to the work.
† Corresponding authors.

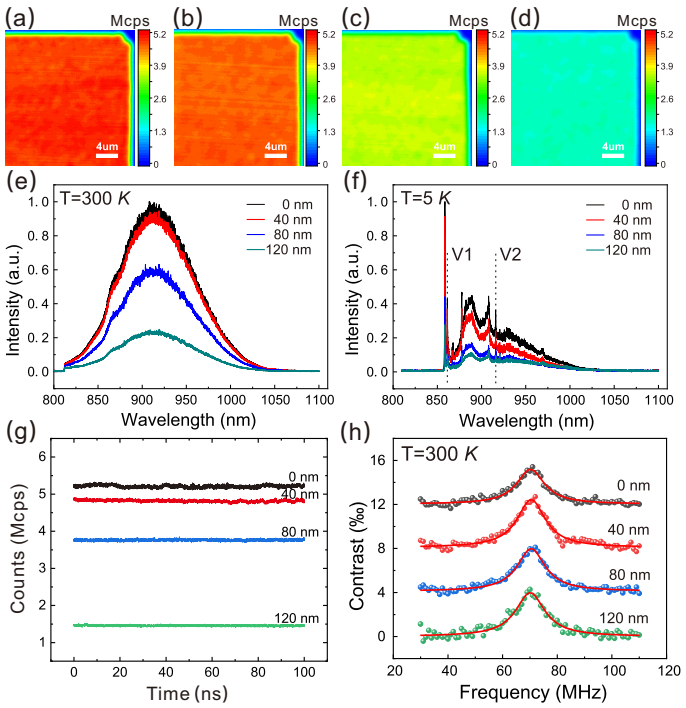

Fig. S1 Depth dependence of PL and ODMR spectrums of V_{Si} defects generated by 20 keV He^+ ions with a dose of 2×10^{13} cm^{-2}. (a)-(d) Fluorescence images at the same position after different etched depths of 0 nm, 40 nm, 80 nm and 120 nm, respectively. (e) The RT PL spectrum of the V_{Si} defects after different etched depths. (f) The LT (5 K) PL spectrum of the V_{Si} defects after different etched depths. Two characterized peaks labeled as $V1$ (861 nm) and $V2$ (915 nm), which are denoted by vertical black dashed lines, correspond to the ZPLs of two types of V_{Si} defects in SiC. (g) The time traces of PL intensity with sampling bin $\delta t = 10ms$, obtained from the V_{Si} defects in the samples after different etched depths at room temperature. (h) The RT ODMR signals of the V_{Si} after different etched depths. The red solid lines are the Lorentz fitting to the data.

ures S2(a) and S2(b), respectively. The two characterized ZPLs of $V1$ (861 nm) and $V2$ (915 nm) according to the two types of V_{Si} defects in SiC are obviously demonstrated in LT PL spectrum [1–4]. Figure S2(c) shows the ODMR spectrum of the V_{Si} defects at room temperature. Inferred from the fitting of the ODMR data, the resonant frequency is 69.8 MHz and the FWHM is 13.5 MHz, which agree with previous results [1,4].

2 Detailed information for the Gaussian distribution fitting

The normalized mean PL intensity of the shallow V_{Si} defects generated by ion implantation versus the etched depth of SiC sample can be obtained by tracing the mean PL intensity of the remaining V_{Si} defects after each etching step. It is assumed that the depth distribution of the V_{Si} defects in SiC sample generated by ion implantation is obeyed by the Gaussian function [5], shown in Equation (1).

$$G(x,\mu,\sigma) = A\cdot exp\left[\frac{(x-\mu)^2}{2\sigma^2}\right], \qquad (1)$$

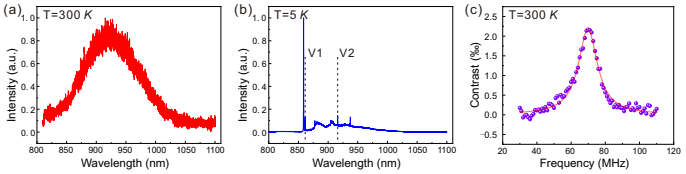

Fig. S2 PL and ODMR spectrums of V_{Si} defects generated by 20 keV H_2^+ ions with a dose of 2×10^{13} cm^{-2} before etching. (a) The RT PL spectrum of the V_{Si} defects, (b) The LT (5 K) PL spectrum of the V_{Si} defects. Two characterized peaks labeled as $V1$ (861 nm) and $V2$ (915 nm), which are denoted by vertical black dashed lines, correspond to the ZPLs of two types of V_{Si} defects in SiC. (c) The ODMR signals of the V_{Si} at room temperature. The red solid line is the Lorentz fitting to the data.

where, A is a normalization constant, μ represents the mean depth of the V_{Si} defects and σ represents the standard deviation value of the depth distribution. In order to deduce the Gaussian distribution function, a normalized Gaussian complementary error function, described as Equation (2), is used to fit the experimental results.

$$f(x,\mu,\sigma) = \frac{\int_x^{\infty} G(x,\mu,\sigma)\,dx}{\int_0^{\infty} G(x,\mu,\sigma)\,dx}\,. \qquad (2)$$

From the fitting, the mean value (μ) and standard deviation (σ) of the depth distribution of V_{Si} defects in SiC sample can be deduced and thus the Gaussian distribution function can be uniquely determined.

3 Depth distribution of V_{Si} defects in SiC simulated by SRIM

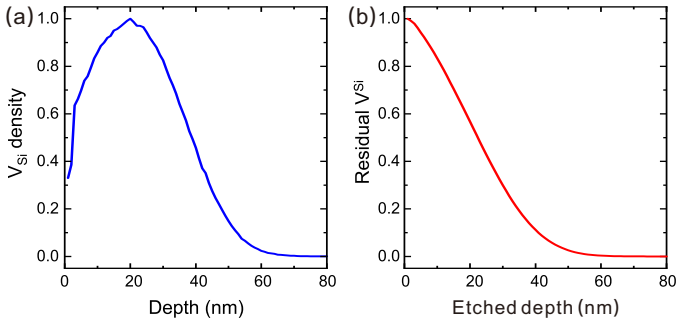

Fig. S3 The depth distribution of V_{Si} defects in the SiC samples implanted by 4 keV He^+ ions. (a) Normalized depth distribution. (b) Normalized residual number of V_{Si} defects in the samples versus different etched depths.

In Figure S3(a), the blue solid line represents the normalized depth distribution of V_{Si} defects in the SiC samples implanted by 4 keV He^+ ions. As shown in Figure S3(b), the red solid line represents the normalized residual number of V_{Si} defects in the samples after different etched depths. Those results are simulated by SRIM.

4 Oxide termination of 4H-SiC

SiC is a compound semiconductor whose native oxide is silicon oxide in general, which can be quickly formed on the SiC surface at room temperature and atmosphere similarly to Si [6]. In order

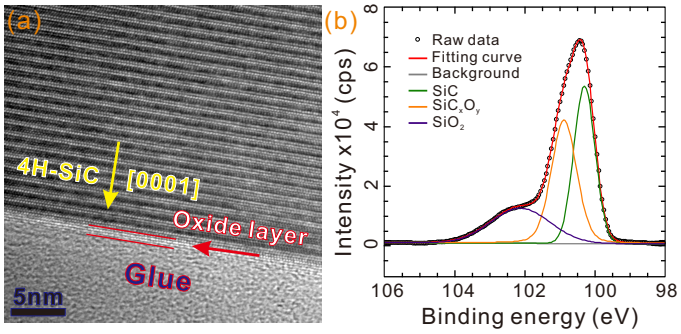

Fig. S4 Oxide termination of the as-received 4H-SiC samples. A representative HRTEM micrograph of the 4H-SiC samples demonstrates a thin oxide layer less than 0.5 nm on its surface. The XPS data of Si 2p shows a typical peak of 4H-SiC surface with native oxide, which can be deconvoluted into three components: SiC, SiC_xO_y, SiO_2.

to verify the thickness of the oxide layer of our 4H-SiC sample, we apply the high resolution transmission electron microscopy (HRTEM, Tecnai G2 F20 S-Twin). Figure S4(a) demonstrates a representative HRTEM micrograph of the as-received 4H-SiC sample with amplification factor of 6.9×10^5 times. An amorphous oxide layer is seen at the interface, which separates the direct contact between glue and SiC. The thickness of the thin oxide layer is less than 0.5 nm. This is a typical native oxide layer, which is consistent with previous results [7,8]. As shown in Figure S4(b), the X-ray photoelectron spectroscopy (XPS, Thermo ESCALAB 250Xi) data of Si 2p shows a typical peak of 4H-SiC surface with native oxide, which can be deconvoluted into three components: SiC, SiC_xO_y, SiO_2. Those peaks are consistent with previous reports [7]. The SiC peak originates from Si emitters, which are located within the SiC substrate and have four bonds to carbon atoms. The SiO_2 peak is ascribed to silicon emitters with four bonds to oxygen atoms. The SiC_xO_y peak is from silicon atoms bonded to both oxygen and carbon atoms. The peak of SiO_2 is weak in this sample, which indicates that the native oxide has no long-rang order yet [8].

References

1 M. Widmann, S. Y. Lee, T. Rendler, N. T. Son, H. Fedder, S. Paik, L. P. Yang, N. Zhao, S. Yang, I. Booker, A. Denisenko, M. Jamali, S. A. Momenzadeh, I. Gerhardt, T. Ohshima, A. Gali, E. Janzén and J. Wrachtrup, *Nat. Mater.*, 2015, **14**, 164–168.

2 M. Radulaski, M. Widmann, M. Niethammer, J. L. Zhang, S. Y. Lee, T. Rendler, K. G. Lagoudakis, N. T. Son, E. Janzén, T. Ohshima, J. Wrachtrup and J. Vučković, *Nano Lett.*, 2017, **17**, 1782–1786.

3 T. C. Hain, F. Fuchs, V. A. Soltamov, P. G. Baranov, G. V. Astakhov, T. Hertel and V. Dyakonov, *J. Appl. Phys.*, 2014, **115**, 133508.

4 F. Fuchs, B. Stender, M. Trupke, D. Simin, J. Pflaum, V. Dyakonov and G. V. Astakhov, *Nat. Commun.*, 2015, **6**, 7578.

5 F. F. de Oliveira, S. A. Momenzadeh, Y. Wang, M. Konuma, M. Markham, A. M. Edmonds, A. Denisenko and J. Wrachtrup, *Appl. Phys. Lett.*, 2015, **107**, 073107.

6 F. Amy, P. Soukiassian, Y. K. Hwu and C. Brylinski, *Phys. Rev. B.*, 2002, **65**, 165323.

7 W. Huang, S. H. Chang, X. C. Liu, B. Shi, T. Y. Zhou, X. Liu, C. F. Yan, Y. Q. Zheng, J. H. Yang, E. W. Shi, W. H. Zhang and J. F. Zhu, *Appl. Phys. Exp.*, 2012, **5**, 105802.

8 M. Schürmann, S. Dreiner, U. Berges and C. Westphal, *Phys. Rev. B.*, 2006, **74**, 035309.